electronics

MDPI

Article

Local Partial Signal Combining Schemes for Cell-Free Large-Scale MU-MIMO Systems with Limited Fronthaul Capacity and Spatial Correlation Channels

Amr A. Alammari[1]*, Mohd Sharique [1], Athar A. Moinuddin[1], and **Mohammad Samar Ansari[2]**

[1] Department of Electronics Engineering, Zakir Hussain College of Engineering & Technology, Aligarh Muslim University, Aligarh 202002, India.
[2] Faculty of Science and Engineering, University of Chester, Parkgate Road, Chester CH1 4BJ, United Kingdom.

* Correspondence: alammari.amr.rs@gmail.com;

Abstract: Cell-Free Large-Scale Multi-user MIMO is a promising technology for the 5G-and-beyond mobile communication networks. Scalable signal processing is the key challenge in achieving the benefits of cell-free systems. This study investigates a distributed approach for Cell-Free deployment with user-centric configuration and finite fronthaul capacity. Moreover, the impact of scaling the pilot length, the number of access points (APs), and the number of antennas per AP on the achievable average spectral efficiency is investigated. Using dynamic cooperative clustering (DCC) technique and large-scale fading decoding process, we derive an approximation of the signal-to-interference-plus-noise ratio in the criteria of two local combining schemes: Local-Partial Regularized Zero Forcing (RZF) and Local Maximum Ratio (MR). Results indicate that distributed approaches in the Cell-Free system have advantages in terms of decreasing the fronthaul signaling and the computing complexity. Among all the distributed combining schemes, the results show that the Local-Partial RZF provides the highest average spectral efficiency. The reason is that the computational complexity of the Local-Partial RZF is independent of the UTs, so it does not grow as the number of user terminals (UTs) increase.

Keywords: Large-Scale MIMO; User-Centric; Cell-Free, MU-MIMO; RZF; LSDF; DCC.

1. Introduction

Fifth-generation (5G) and beyond technology has been developed to meet the constant demand for reliable wireless services with higher data rates [1]. It is projected that 5G-and-beyond systems will be able to connect and mange unprecedented number of devices and provide ubiquitous services [2]. To address the design challenges of 5G-and-byond, several key technologies are being investigated [3]-[11]. Some of the candidate technologies that proposed for the 5G-and-beyond mobile communication networks include, reconfigurable intelligent surface [4], SLNR-based beamforming [6], millimeter wave [7],[8], advanced multiple access [9],[11], and Large-Scale Multi-user Multiple Input Multiple Output (MU-MIMO). Due to its ability to minimize the interference, Large-Scale MU-MIMO can provide several orders of magnitudes of improvement the system spectral efficiency.

A recently developed concept, known as Cell-Free Large-Scale MU-MIMO, provides a novel network architecture based on three well-known technologies: Large-Scale MU-MIMO [12]-[18], Coordinated Multi-Point (CoMP) [19], and Distributed Antenna System (DAS) [20], [21]. Cell-Free Large-Scale MU-MIMO has been proposed as a potential alternative to dividing up the coverage area into cells.

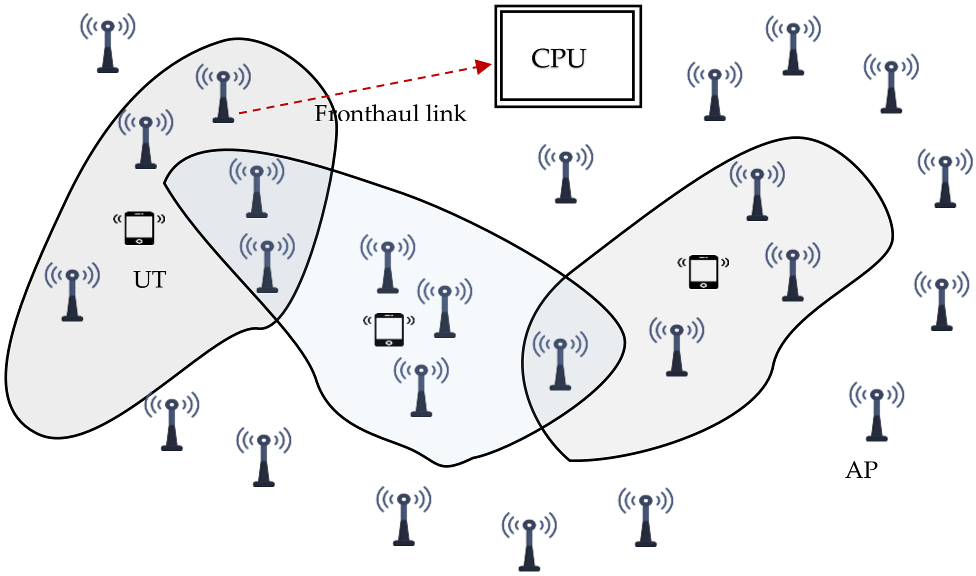

Figure 1: User-Centri Cell-Free system with dynamic cooperative clustering

Compared to the conventional cellular network layout, Cell-Free network layout eliminates the cell borders and the resulting inter-cell interference [22], [23]. In the Cell-Free system, a large number of access points (AP), which distributed in the area of coverage, provide services to a large number of users. All APs in this system deployment use fronthaul links to communicate with a central processing unit (CPU). The CPU manages and coordinates all the transmissions in the network.

There are typically two implementation approaches for Cell-Free systems [24]-[27]: completely centralized, and distributed. In the centralized approach, all signal processing is performed at the CPU. All APs forward the received pilot and data signals to the CPU, which will carry out the necessary processing. Taking into account the practical constraints of having links with limited fronthaul capacity, this approach typically leads to unmanageable fronthaul signaling.

In the distributed Cell-Free implementation, the required signal processing is shared between the CPU and the APs, and depending on the amount of this sharing, different levels of distribution can be accomplished. The initial concept for Cell-Free is developed on the basis of two primary assumptions: all the active UTs in the network are served by all the APs simultaneously [28], [29], and availability of unlimited capacity for the fronthaul links [30], [31].

In Large-Scale MU-MIMO, the maximum sum spectral efficiency (SE) that can be achieved is constrained by two factors: wireless channel capacity and fronthaul link capacity [32]. The distributed approach can be used to achieve reduction in the fronthaul requirements [33]. In this architecture, some baseband signal processing is done at the APs. As a result of this motivation, the system uplink performance with limited fronthaul capacity and different local distributed combining schemes is considered. The distributed implementation adopted in this paper is distinguished from the centralized implementation by the following:

1) channel estimation process is performed locally at each access point;
2) Combiner design and data estimation are performed locally at each access point;
3) APs use the fronthaul links to send the data estimates only;
4) An additional stage of data estimation is performed centrally by the CPU.

1.1. Related Work

Recently, Cell-Free systems have attracted a great deal of interest, and many previous studies have evaluated their performance from a variety of perspectives [22],[24], [26]-[45]. For instance, in [22], the sum spectral efficiency for Maximum Ratio beamforming/combining has been derived. A stochastic geometry technique was employed in [34] to evaluate the system performance. Additionally, [36] studied a Cell-Free system with power optimization and precoding technique to enhance the network data rate. The fully centralized approach of Cell-Free system, in which the estimation process and combiner design are performed centrally, is investigated in [27], [37]. Distributed implementations are considered in [38] in order to reduce the fronthaul traffic.

In order to make the analysis more manageable, most of the previous studies consider a wide variety of simplifying assumptions, including the following:

- *All users are served by all APs in the same time-frequency resource:* For example, authors in [39] investigated the achievable uplink rate performance of the Cell-Free systems with perfect/imperfect CSI and Zero Forcing (ZF) processing. However, in practice and as a result of this assumption, the system will not be scalable, implying that the system will be unable to manage an increasing number of active UTs and APs. Also, this configuration is impractical since only a limited number of APs can beneficially communicate with a particular UT. To address these constraints and maintain scalability, we consider a practical system configuration which allows UTs to dynamically choose their subset of APs. Thus, a group of nearby APs are cooperatively serving each UT, as shown in Figure 1. In this user-centric configuration, a clustering technique known as Dynamic Cooperative Clustering (DCC) is used, which allows UTs to choose their preferred set of serving APs. With the DCC approach, the scalability comes from the fact that only the UT's corresponding subset of APs will be involved in the signal processing. The works in [40], [41] have investigated a user-centric configuration for Cell-Free systems with different channel estimators. However, these studies are based on simple beamforming/combining schemes with some idealized assumptions.

- *Unlimited fronthaul/backhaul link capacity*: For example, the authors in [42] investigate the downlink of a Cell-Free system considering power control technique and ZF process. However, each fronthaul/backhaul connection will have a finite capacity when dealing with practical systems. Moreover, to achieve scalability, it is necessary to restrict the fronthaul signaling that occurs between the APs and the CPU. The authors in [43] investigated the impact of using capacity constrained fronthaul links on the average max-min rate per user, considering low-complexity hybrid precoders/decoders. However, the study focuses on the centralized case where the baseband processing of the transmitted signals is fully performed at the CPU. We investigate the uplink of a cell-free Large-Scale MU-MIMO system with distributed implementation, limited fronthaul links, and DCC approach.

- *The propagation channels are spatially uncorrelated*: For example, studies in [44], [45] analysed the system performance under independent Rayleigh channels using general models such as uncorrelated Rayleigh fading. However, in practice, the correlation between the antenna elements is inherent in the implementation of the Cell-Free System due to the large number of APs. For realistic performance investigation of Cell-Free systems, a physical correlated channel model is considered in this paper.

1.2. Contributions

By investigating the local distributed user-centric approach of a Cell-Free system with finite fronthaul links Capacity, the main contributions of our work include the following:

- *Uplink System modeling*: In this paper, we consider the uplink scenario of a user-centric Cell-Free system with finite capacity fronthaul links to investigate the impact of distributing the signal processing between the APs and the CPU for achieving a certain level of performance. The distributed system implementation is modeled and numerically simulated. The goal of this research is to provide a further understanding of partial local distributed Cell-Free systems under more realistic system considerations.
- *Analysis of distributed implementations for user-centric Cell-Free system:* Two system configurations, namely, local distributed, and two-stage distributed are considered to study how competitive these configurations are to a centralized-based system configuration vis-à-vis the achieved SE. Extensive simulations have been performed to evaluate the system's performance from different perspectives, including the effect of increasing the pilot length, APs number, and APs' antennas, for the three schemes: Partial RZF, Local-partial RZF, and Distributed MR.
- *Distributed Physical layer processing*: The essential local physical layer procedures in the distributed user-centric Cell-Free uplink transmission, such as pilot signaling, channel estimation, and data detection, are identified. Using different bounding techniques, we derive an approximation for the effective SINR using the clustering concept and the large-scale fading decoding (LSFD)scheme.

1.2. Paper Organization

The remaining parts of this work are structured as follows: The user-centric Cell-Free Large-Scale MU-MIMO system model is described in Section 2. In Section 3, computational complexity and fronthaul signaling are analyzed. In Section 4, a physical geometric-based channel model which is considered in this paper is presented. Simulation results and discussion are presented in Section 5, followed by concluding remarks in Section 6.

2. System Model

We consider a Cell-Free system with K single-antenna user terminals (UTs) which are served by L access points (APs) and all the UTs and the APs are distributed randomly in the coverage area. Let N be the number of antennas per AP. The system satisfies the user-centric condition, where a set of APs, $\mathcal{Q}_k \subset \{1,2,\dots\dots,L\}$ cooperate to serve an arbitrary UT k. Also, we consider a block fading model, where all the channels are considered to be static and frequency flat within a single block (known as the coherence block) and vary among different blocks.

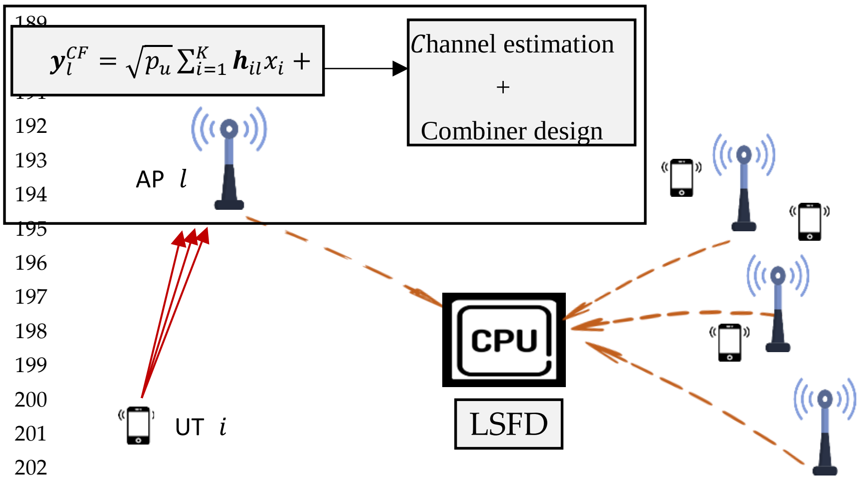

Figure 2: Local Distributed Operations considered in this work

The coherence block size is determined by many factors, including carrier frequency, mobility, propagation environment, and so on. Further, in this block fading model, each coherence block is divided into τ_{p} channels used for the uplink pilot training, τ_{u} for sending data on the uplink, and τ_{d} channels for sending the data on the downlink. Let $\mathbf{h}$ denotes the channel response between the k^{th} UT and the L^{th} AP, and the channel realization is drowned from an independent correlated Rayleigh fading distribution as

$$\mathbf{h}_{kl} \sim \mathcal{N}_C\,(0, \boldsymbol{R}_{kl}) \qquad (1)$$

where $\mathbf{R}$ represents the spatial correlation matrix, which contains the small-scale fading as well as the large-scale fading. In the block fading model, the small-scale effect can be static in one coherence block, and it may change among different blocks. On the other hand, the effect of large-scale fading is considered to be changing more slowly and can be regarded as constant for a number of coherence blocks.

We consider the distributed implementation given in Figure 1, and the operations of interest in this paper include uplink training, channel estimation, combiner design, and data detection.

2.1. Uplink Training and Channel estimation

In the training stage, all the UTs send their pilots to the APs throughout a pilot-based training process. The training pilots are known as the pilot sequence and the network is assumed to have τ_{p} available orthogonal pilot sequences. However, it is expected that the number of active UTs will be more than the number of available orthogonal sequences ($K > \tau_{\mathrm{p}}$). This will make several UTs to reuse the same pilot sequences in their analyses. The term "pilot contamination" refers to a problem that occurs in the Large-Scale MU-MIMO networks when multiple UTs use the same pilot sequences. The received pilot signal at the AP l can be given as

$$\mathbf{y}_l^{pilot} = \sqrt{p_p}\sum_{i=1}^{K} \boldsymbol{h}_{il}\,\boldsymbol{\psi}_{t_i}^{H} + \boldsymbol{W}_l \qquad (2)$$

where p_p is the transmitted pilot power, $\boldsymbol{W}_l$ is the additive independent white Gaussian noise matrix with independent and identically distributed $\mathcal{N}\,(0, \sigma^2)$ elements, $\boldsymbol{\psi}_{t_i}^{H}$ is the pilot sequence sent by the k^{th} UT and $t = 1, \ldots\ldots, \tau_{\mathrm{p}}$.

Based on the received pilot signal in (2), the AP l performs the channel estimation process. The LMMSE estimator is employed in each AP to estimate the channel coefficients to the UTs. The estimated channel between the UT k, and the AP l is given as [46]

$$\widehat{\boldsymbol{h}}_{il} = \sqrt{p_p \tau_p} \mathbf{R}_{il} \boldsymbol{Q}_{corr}\, \boldsymbol{y}_{tl}^{pilot} \tag{3}$$

where $\mathbf{R}_{il}$ denotes the spatial correlation matrix, $i \in \mathcal{Q}_k$, and $\mathbf{Q}_{\text{corr}}$ denotes the inverse of the normalized correlation matrix.

The different between the channel and its estimate is known as the estimation error, and can be termed as $\boldsymbol{e}_{il} = \boldsymbol{h}_{il} - \widehat{\boldsymbol{h}}_{il}$. The covariance matrices of both $\widehat{\boldsymbol{h}}_{il}$ and $\boldsymbol{e}_{il}$ for the cell-Free distributed implementation can be given as follows

$$\mathbf{C}_{\text{est.}} = p_p \tau_{\text{p}} \mathbf{R}_{il} \mathbf{Q}_{corr}\, \mathbf{y}_{tl}^{pilot} \mathbf{R}_{il} \tag{4}$$

$$\mathbf{C}_{\text{err.}} = \mathbf{R}_{il} - p_p \tau_{\text{p}} \mathbf{R}_{il} \mathbf{Q}_{corr}\, \mathbf{y}_{tl}^{pilot} \mathbf{R}_{il} \tag{5}$$

In the distributed implementation and in contrast to the analysis for the centralized implementation, the channels statistics from UT k to its connected APs will be used locally at each AP for designing the combiner and to estimate the transmitted signal.

2.2. Combiner design and signal detection

After the channels are estimated locally at the APs, the UTs transmit their data symbols. The received signals are processed at each APs to detect the desired signal $\hat{x}_k$. The detection process in the distributed approach involves two stages of data estimation:

First, based on (2), the transmitted signals can be estimated locally at the APs by applying a linear combiner as

$$\hat{x}_{l,k} = \boldsymbol{a}_{l,k}\, \boldsymbol{y}_l^{CF} = \boldsymbol{a}_{l,k}^H \boldsymbol{h}_{l,k} x_k + \sum_{\substack{i=1 \\ i \neq k}}^{K} \boldsymbol{a}_{l,k}^H \boldsymbol{h}_{l,i} x_i + \boldsymbol{a}_{l,k}^H \boldsymbol{w}_l \tag{6}$$

where $\boldsymbol{a}_{l,k}$ represents the combiner that is containing vectors from all APs that communicate with the UT k. Note that the detection process in the user-centric approach is constrained to a subset of APs (i.e., $\mathcal{Q}_k \subset \{1,2, \dots \dots, L\}$) corresponding to the UT k.

Then, based on (6), another stage of signal estimation is performed centrally by the CPU. This process is known as large-scale fading decoding (LSFD), which involves using LSFD weight vector $\{\mathbf{v}_{l,k} : l = 1, \dots, L\}$ to estimate the data symbols as

$$\hat{x}_k = \sum_{l=1}^{L} \boldsymbol{v}_{l,k}^* \, \hat{x}_{l,k}$$

$$\hat{x}_k = \sum_{l=1}^{L} \boldsymbol{v}_{l,k}^* \, \boldsymbol{a}_{l,k}^H \boldsymbol{h}_{l,k} x_k + \sum_{l=1}^{L} \boldsymbol{v}_{l,k}^* \, \boldsymbol{a}_{l,k}^H \sum_{\substack{i=1 \\ i \neq k}}^{K} \boldsymbol{h}_{l,i} x_i + \sum_{l=1}^{L} \boldsymbol{v}_{l,k}^* \, \boldsymbol{a}_{l,k}^H \boldsymbol{w}_l \tag{7}$$

In general, the ergodic capacity of the Large-Scale MU-MIMO system has not yet been defined. However, different bounds on the capacity are available. These bounds are also known as achievable SE and can be used to evaluate the system performance. In this paper, a lower bound technique is used to study the uplink system performance with local distributed combing schemes. Following the same argument in [33], the uplink achievable SE of UT k for user-centric Cell-Free system can be given as

$$SE_k^{CF} = \left(1 - \frac{\tau_p}{\tau_c}\right) \mathbb{E}\left\{ log_2 (\, 1 + SINR_k^{CF}) \right\} \tag{8}$$

where SINR is the effective signal to interference and noise ratio, which can be given as

$$SINR_k = \frac{p_k \left| \boldsymbol{v}_k^H \mathbb{E}\{\boldsymbol{g}_{k,k}\} \right|^2}{\sum_{i=1}^{K} p_i \mathbb{E}\left\{ \left| \boldsymbol{v}_k^H \boldsymbol{g}_{i,k} \right|^2 \right\} - p_k \left| \boldsymbol{v}_k^H \mathbb{E}\{\boldsymbol{g}_{k,k}\} \right|^2 + \sigma^2 \boldsymbol{v}_k^H \boldsymbol{F}_k \boldsymbol{a}_k} \tag{9}$$

It is to be noted that the capacity bound in (8) can be used for many channel fading distributions. The expression in (9) has deterministic terms which can be calculated due to the fact that the transmitted signal can be identified as if it was transmitted via AWGN channel with gain $\mathbb{E}\{\boldsymbol{a}_{l,k}^H \boldsymbol{D}_{l,k} \boldsymbol{h}_{l,k}\}$.

By employing the DCC concept where the $\boldsymbol{a}_{l,k}^{H}$ in (7) can be replaced with $\boldsymbol{a}_{l,k}^{H}\boldsymbol{D}_{l,k}$ and select the LSFD vector $\mathbf{v}_k$ as $\boldsymbol{v}_k = p_k\left(\sum_{i=1}^{K} p_i \left\{\boldsymbol{g}_{i,k}\boldsymbol{g}_{i,k}^{H}\right\} + \sigma^2\boldsymbol{F}_k\right)$, the expression in (9) can be further maximized. Hence, the maximized $SINR$ can be written as

$$SINR_k^{max} = p_k\{\boldsymbol{g}_{k,k}^{H}\} \times \left(\sum_{i=1}^{K} p_i \left\{\boldsymbol{g}_{i,k}\boldsymbol{g}_{i,k}^{H}\right\} + \sigma^2\boldsymbol{F}_k - p_k\mathbb{E}\left\{\boldsymbol{g}_{k,k}\right\}\mathbb{E}\left\{\boldsymbol{g}_{k,k}^{H}\right\}\right)^{-1}\{\boldsymbol{g}_{k,k}\} \tag{10}$$

where , $\boldsymbol{D}_k = dig\left(\boldsymbol{D}_{1,k}, \ldots, \boldsymbol{D}_{1,k}\right)$, $\mathbf{g}_{i,k} = [\boldsymbol{a}_{1,k}^{H}\boldsymbol{D}_{1,k}\boldsymbol{h}_{1,k}, \ldots\ldots, \boldsymbol{a}_{L,k}^{H}\boldsymbol{D}_{L,k}\boldsymbol{h}_{L,k}]^{\mathrm{T}}$, and $\boldsymbol{F}_{\mathrm{k}} = dig\left(\left\{\left\|\boldsymbol{D}_{1,k}\boldsymbol{a}_{1,k}^{H}\right\|\right\}, \ldots\ldots, \left\{\left\|\boldsymbol{D}_{L,k}\boldsymbol{a}_{L,k}^{H}\right\|\right\}\right)$.

In the combiner design process, the vector that maximizes the effective SINR in (8) is the optimal combiner. To maximize the effective SINR, we consider two scalable combining schemes: Local-Partial Zero-Forcing-based, and Local MR-based.

In the presence of inter-user interference, ZF-based schemes provide better performance as compared to MR schemes. The Local-Partial RZF combining for UT k at AP l can be expressed as

$$\boldsymbol{a}_{l,k}^{LPRZF} = p_k\left(\sum_{i \in D_l} p_i \widehat{\boldsymbol{h}}_{il}\widehat{\boldsymbol{h}}_{il}^{H} + \sigma^2 I_{N_{AP}}\right)^{-1}\boldsymbol{D}_{kl}\widehat{\boldsymbol{h}}_{kl} \tag{11}$$

The Local-Partial RZF vectors from all APs that serve the UT k can be written in a matrix form as

$$\boldsymbol{A}_{l,k}^{\boldsymbol{LPRZF}} = \boldsymbol{D}_{kl}\widehat{\boldsymbol{H}}_{D_l}\left(\widehat{\boldsymbol{H}}_{D_l}\widehat{\boldsymbol{H}}_{D_l}^{H} + \sigma^2\boldsymbol{P}_{D_l}^{-1}\right)^{-1} \tag{12}$$

where all the vectors of $\widehat{\boldsymbol{h}}_{il}$, with the indices $i \in D_l$, are staked together and form the matrix $\widehat{\boldsymbol{H}}_{D_l}$. All the transmit powers p_i for $i \in D_l$ are contained in a diagonal matrix $\mathbf{P}$.

After the Local-Partial RZF detection process, all signals are forwarded to the central unit over fronthaul links. Then, another stage of signal detection is performed by the CPU, which applies the LSFD scheme and detect the desired signal. By substituting (12) into (10), the average sum SE of UT k is obtained by (8).

The MR combining vector can be expressed as

$$\boldsymbol{a}_{l,k}^{\boldsymbol{MR}} = \boldsymbol{D}_{l,k}\widehat{\boldsymbol{h}}_{l,k} \tag{13}$$

MR combiner maximizes the receive power and neglect the inter-user interference. To suppress the inter-user interference, sophisticated combining schemes are used.

3. Computational complexity and fronthaul signaling

This section presents a detailed analysis of the basic tradeoffs between maintaining improvement in the performance and the increase in the computational complexity. Using the technique propounded in [17], which was proposed for cellular networks, the computational complexity of different distributed schemes in Cell-Free system will be evaluated and compared with that of centralized schemes. The key advantage of using alternative combining methods than MMSE-based approaches is the reduction in the computational complexity. Local ZF-based schemes are more practical in terms of minimizing the computational complexity and the amount of channel statistics required to design the combining vector. Combining schemes that achieve higher SEs have higher computational complexity. Hence, a reduction in complexity comes with the cost of decreasing the SE.

Counting the required complex multiplications and divisions is one way to quantify the computational complexity in the Large-Scale MU-MIMO. For example, for a correlation matrix $\mathbf{R} \in \mathbb{C}^{N_1 \times N_2}$, the required number of complex multiplications for $\mathbf{R} \times \mathbf{R}^{\mathrm{H}}$ is given as

$$\text{No. of complex multiplications} = \left((N_1^2 + N_1)/2\right)N_2 \tag{14}$$

If the multiplication carried out with different matrix, for example $\mathbf{Q} \in \mathbb{C}^{N_2 \times N_3}$; the $\mathbf{R} \times \mathbf{Q}$ multiplication needs $N_1 \times N_2 \times N_3$ complex multiplications.

The downside of centralized implementation is that the digital baseband processing system in the CPU has to process all the signal observations forwarded by all the APs. The channel estimates that are utilized in the combining process are computed at the CPU for all UTs. However, in the distributed implementation the channel estimates are computed at each AP once per coherence block for each corresponding UT. When the computational complexity per UT of a combining scheme is independent of K, it known as a scalable scheme. The received combining schemes considered in Section 3 are scalable schemes, i.e. they exhibit a finite complexity as $K \to \infty$.

In the local distributed MR scheme given in (13), the required number of complex multiplications for estimating the channels can be written as

$$(N_{\tau_p} + N^2)|\mathcal{Q}_k| \tag{15}$$

Here, we are considering the case of using the MR combining along with the LSFD. For the Local-Partial RZF scheme given in (11), the number of the required complex multiplications can be given as

$$(N_{\tau_p} + N^2)\ \sum_{i\in\mathcal{Q}_k}|\mathcal{D}_l| \tag{16}$$

Compared to the corresponding centralized schemes, the distributed MR scheme with LSFD is equivalent to the centralized MR [33]. However, for the ZF-based schemes, the distributed Local-Partial RZF has a lower complexity as compared to the centralized Partial RZF. The reason is that the distributed operation in the Local-Partial RZF involves computing only the inverse of $N \times N$ matrix.

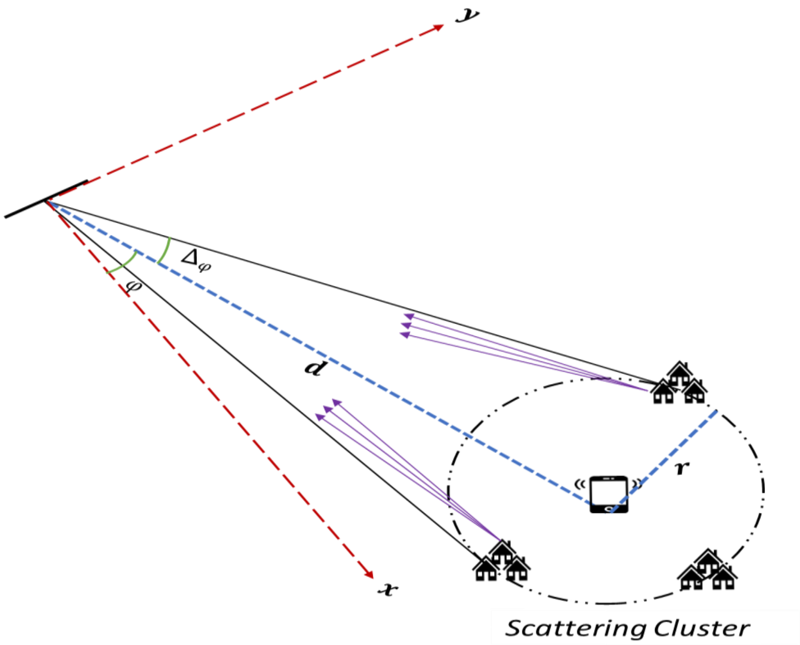

Figure 3: 3-D physical channel model, where the scatterers distributed around the user terminal (UT). Each path characterized by two angles: the azimuth (φ_i) and elevation (θ_i).

4. Spatial Correlation Model

In this section, the spatial correlation matrix $\mathbf{R}_\mathcal{X}$ is generated using a physical geometric-based stochastic channel model. This channel modeling accounts for several channel aspects, including, antenna correlation, geometric characteristics of the antenna elements and the scatterers, and the UTs' locations. Assuming that the scattering process happens only in proximity of the UTs, a 3-D Gaussian Local Scattering scheme is assumed in this study. In this scheme, signals from different paths $(\mathcal{Z})$ reach the APs, and the correlation matrix can be given as [47]

$$\boldsymbol{R}_{\chi} = \mathbb{E}\left\{\sum_{i=1}^{Z} \boldsymbol{\alpha}_i \boldsymbol{\alpha}_i^H\right\} \quad (17)$$

where $\boldsymbol{\alpha}_i$ denotes the array response of i^{th} path and can be redefined as a function of the azimuth (φ_i) and elevation (θ_i) angles as

$$\boldsymbol{\alpha}_i = \boldsymbol{\alpha}(\varphi_i, \theta_i) \quad (18)$$

For a particular (l, m) element, $\mathbf{R}_{\chi}$ can be given as,

$$[\boldsymbol{R}]_{l,m} = \beta \int\int e^{j\pi(m-l)sin(\bar{\varphi})cos(\bar{\theta})} f(\bar{\varphi}, \bar{\theta}) d\bar{\varphi} d\bar{\theta} \quad (19)$$

where β denotes the large-scale fading coefficient for the i^{th} multipath component which arrives from a certain azimuth angle $\bar{\varphi}$, and a certain elevation angle $\bar{\theta}$, while $f(\bar{\varphi}, \bar{\theta})$ is the PDF of $\bar{\varphi}$ and $\bar{\theta}$.

In the considered scheme and similar to [48], the scatterers are distributed in a Gaussian distribution, and hence the $\mathbf{R}_{\chi}$ is rewritten as

$$[\boldsymbol{R}]_{l,m} = \beta \int\int e^{j\pi(m-l)sin(\bar{\varphi})cos(\bar{\theta})} \frac{1}{2\pi\Delta_{\varphi}\Delta_{\theta}} e^{-\frac{(\bar{\varphi}-\varphi)^2}{2\Delta_{\bar{\varphi}}^2}} e^{-\frac{(\bar{\theta}-\theta)^2}{2\Delta_{\bar{\theta}}^2}} \quad (20)$$

where Δ_{φ}, and Δ_{θ} denote the horizontal and vertical angular standard deviations (ASD) with respect to azimuth and elevation angle, respectively. This model is shown in Figure 3, which illustrates the multipath variations in the azimuth angle.

The horizontal angular ASD defined as

$$\Delta_{\varphi} = \tan^{-1}(r/d) \quad (21)$$

where r and d denote the radius and the horizontal distance. The mean elevation angle and the vertical ASD is defined with respect to the maximum and minimum elevation angles as follows. Maximum elevation angle can be achieved by a scatterer located at a distance $d - r$ and defined as

$$\theta_{max} = \tan^{-1}\frac{h}{d-r} \quad (22)$$

where h denotes the height. Similarly, the minimum elevation angle can be achieved at a distance $d + r$ as

$$\theta_{min} = \tan^{-1}\frac{h}{d+r} \quad (23)$$

Hence, the mean elevation angle and the vertical ASD can be computed as follows

$$\theta = \frac{\theta_{max}+\theta_{min}}{2} \quad (24)$$

$$\Delta_{\theta} = \frac{\theta_{max}-\theta_{min}}{2} \quad (25)$$

5. Numerical Results and Discussion

In this section, a series of Monte-Carlo simulations are carried out to evaluate the distributed implementation of the Cell-Free system. The uplink transmission is considered, and the network is considered to be a suburban environment deployed in an area of 2 Km^2. The UTs and the APs are distributed uniformly at random in the deployed area. For this simulation setup, the key simulation parameters that have been selected are reported in [Table 3, [25]]. The large-scale fading coefficients are given as [46]

$$\beta_{kl}[dB] = A_{d_0} - 10\gamma \ log_{10}\left(\frac{d_{kl}}{d_0}\right) + F_{kl} \quad (26)$$

where A_{d_0} denotes the average channel gain at a reference distance d_0, γ represents the path loss exponent, d_{kl} denotes the distance between the antenna element and the UT, $F_{kl} \sim \mathcal{N}(0, \sigma_{shadow}^2)$ is random variable with zero-mean and variance σ_{shadow}^2, which models the shadowing. The 3-D Gaussian Local Scattering scheme given in Section 4 is used in all the simulations.

Focusing on the system performance with a distributed implementation, two local partial combining schemes are considered to study the benefits of locally performing the channel estimation and the combiner designing at the APs. Next, we consider the LSFD to study the effect of having two stages of data estimation in the Cell-Free system. Then, we investigate the effect of increasing the number of the antennas at the APs. Finally, the computational complexity and the effect of increasing the number of UTs of the distributed schemes is presented. Note that for the sake of comparison, different centralized schemes are presented as a reference in all the simulations.

5.1. Local Partial Distributed implementation

Considering a user-centric approach, Figure 4 and Figure 5 illustrate the system performance and present a comparison of three different implementations: centralized; partial (one stage); and Local partial with LSFD (two stages). It can be seen that the highest average SE is obtained with the centralized approach at the expense of higher fronthaul requirements. However, to decrease the fronthaul requirements, the distributed approach is investigated in this section.

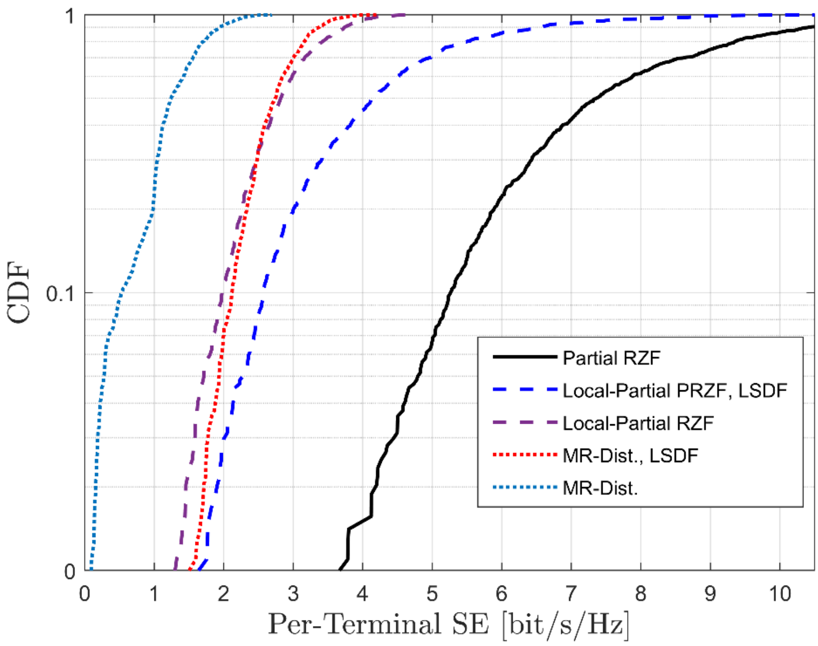

Figure 4: Cumulative Distribution Function (CDF) distribution of for an arbitrary UT as a function of the average achievable SE, with L=256 , K=32, and τ_p=8.

Figure 4 shows the CDF distribution as a function of the achieved average SE. Under the fronthaul constraints, the simulations are carried out for the different system implementations with total active UTs $K = 32$, serving single antenna APs $L = 256$, pilot length $\tau_p = 8$. It can be seen that there exists a significant gap in the performance between the ZF-based and MR-based combining schemes. The is because the MR schemes are unable to suppress the inter-user interference. For instance, Local-Partial RZF scheme gives 43% higher improvement in the average SE. Moreover, it can be observed that the system performance with Local-Partial RZF and MR can be enhanced by adding LSFD scheme as a second detection stage.

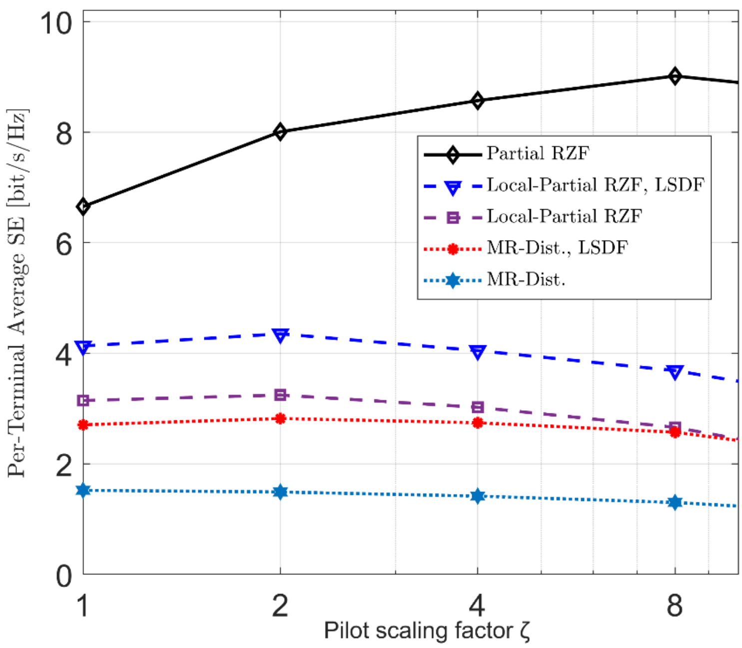

Figure 5: Average achived SE as a function of pilot scaling factor, with K=128, L=1024, and τ_0=8.

Figure 5 illustrates the impact of using higher pilot scalers on the system achievable SE with local distributed detection. Here, we employ a single antenna APs with $K = 128$, and $L = 1024$. In the Cell-Free systems, each AP is allowed to serve up to UTs=τ_p. Let ζ be the scaling factor controlling the pilot length (τ_p), and τ_p given as

$$\tau_p = \zeta \times \tau_0 \tag{27}$$

where, $\tau_0 = L/K$ is the initial pilot length.

It can be observed that increasing the pilot scalers will improve the system performance due the reduction in the pilot reuse, which in turn reduces the pilot contamination. Thus, the average SE continues to increase up to a specific point. Also, different schemes saturated at different points. After these saturated points, any increase in the scaling factor will result in a decrease in the system average achievable SE. Its clear from Figure 5 that '8' and '2' are the saturation points for Partial RZF and MR distributed combining, respectively, while '2' is the same saturation point for Local-Partial RZF and MR-Dist. This is the case when LSFD scheme is employed. However, the two schemes without LSFD are saturated at '2' and '1', respectively.

5.2. Multiple Antennas APs

Considering the achievable SE, Figure 6 and Figure 7 depict the average SE of Partial RZF, Local-Partial RZF, and MR as a function of L. We consider $K = 8$, L increases with a constant rate, and the number of antennas per APs either one (Figure 6) or four (Figure 7).

As can be seen in Figure 6 and Figure 7, a significant improvement in the achievable SE can be obtained for all schemes when L grows higher. This is due to the increase in the diversity gain which increased with L. Also, one can observe that Partial RZF, Local-Partial RZF and Local-Partial RZF with LSFD benefit more as compared to the MR when L grows higher. This is because the ability of ZF-based schemes to minimize the inter-user interference.

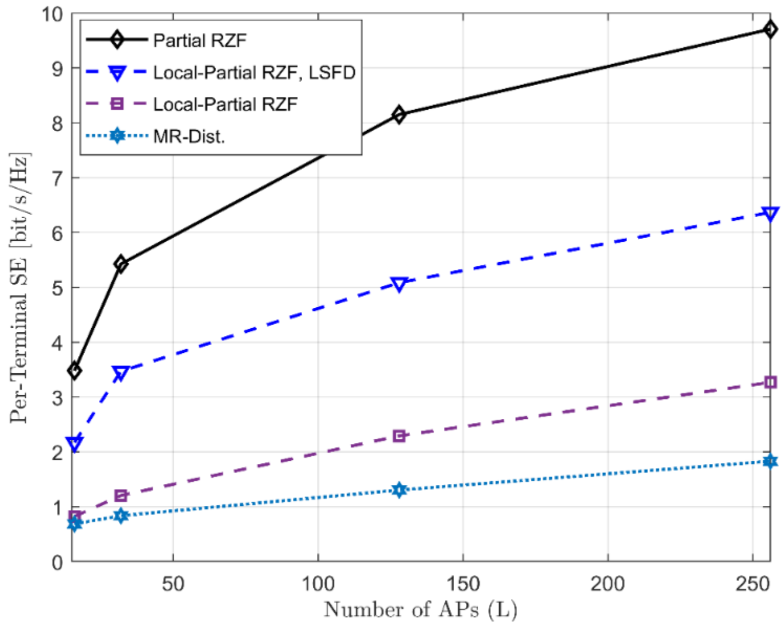

Figure 6: Average achievable SE as a function of L, with K=8, and $\tau_0 = 8$. Each AP is equiped by a single antenna.

Among different local combining schemes in the distributed approach, Local-Partial RZF with LSFD scheme offers the highest achievable SE. Figure 7 shows that deploying each AP with more than one antenna is significantly improve the average achievable SE. The reason is that increasing the number of antennas per AP increases the ability to suppress the different users' interference; and hence the average achievable SE is increased.

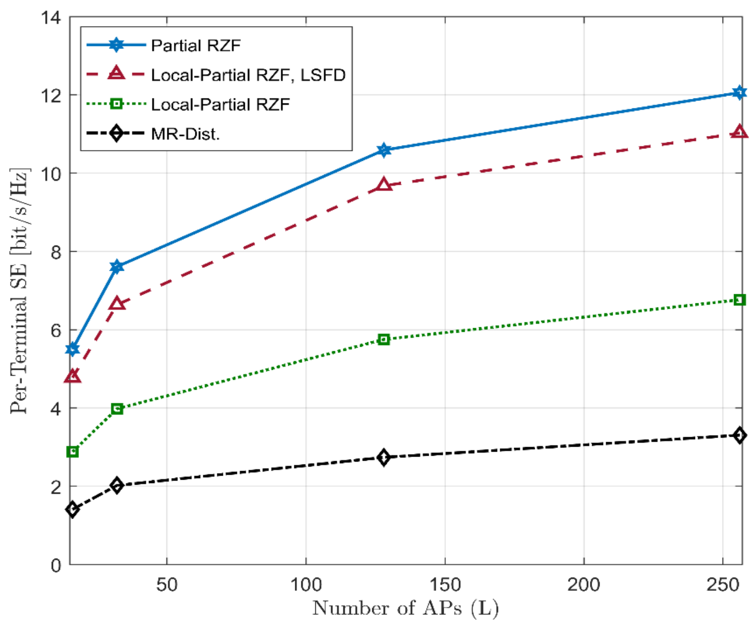

Figure 7: Average achievable SE as a function of L, with K=8, and $\tau_0 = 8$. Each AP equiped by four antennas.

5.3. Computational Complexity

Unlike the centralized-based schemes, the distributed combining schemes have the ability to reduce the amount of interference caused between users in a distributed manner, which implies that the APs perform the estimation, and design the combining vectors locally. Furthermore, the computations of local distributed-based combining schemes have lower complexity than the centralized schemes. This is because the matrix inversion in the local distributed-based schemes has a much smaller dimension.

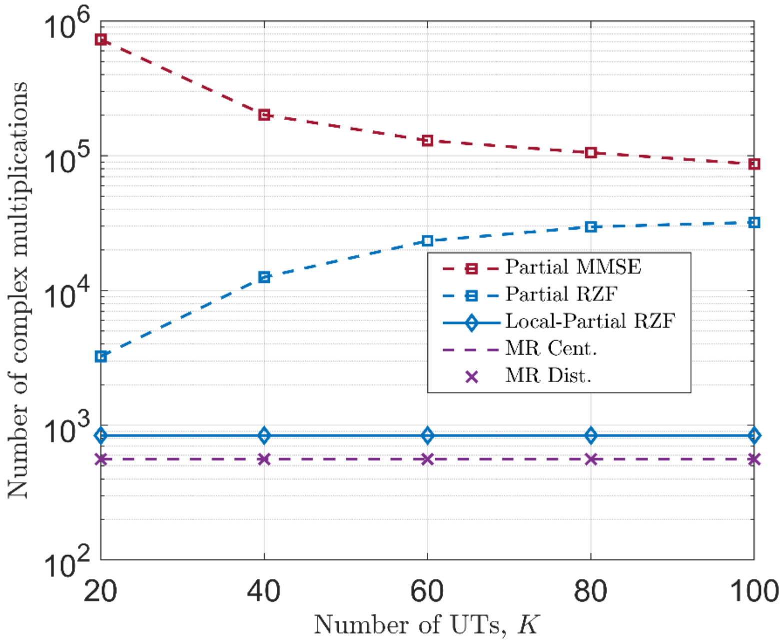

Figure 8: The number of computational complexities as a function of UTs. The total number of ASs in the network L=100, and each AP is equipped with 4 antennas. We consider τ_0=8

Figure 8 shows the complexity in terms of number of complex multiplications as a function of UTs. Among all the five schemes, two of the centralized schemes, namely, Partial MMSE and Partial RZF, have the highest computational complexity. In the case of Partial MMSE using the dynamic cooperative clustering for centralized scheme, the computational complexity decreases as the number of UTs increases [33]. In addition, the partial MMSE is a scalable combining scheme that can be employed with a slight loss in SE; as a benefit of this, a reduction in complexity is observed in figure 8. The Partial RZF has achieved less complexity than Partial MMSE. However, as the number of UTs increases, the computational complexity increases, and the gap between the two schemes decreases. The reason is that in the partial RZF, on average, the number of UTs served by the same group of APS increases as K increases.

For the Local-Partial RZF distributed scheme, it can be observed that the computational complexity is independent of the UTs, so it does not grow as $K \rightarrow \infty$. Despite the fact it has the lowest complexity, MR schemes in both implementations (centralized and distributed) are known to be suboptimal schemes due to its neglecting the existing inter-user interference.

5.4. Discussion

Considering that the proposed scheme entails sharing of the computational load between the CPU and the APs, the Local-Partial RZF distributed scheme would be very suitable for modern 'edge computing', wherein more and more processing is being delegated to the edge devices and being off-loaded from the central processing node (or the cloud)

[49]. There has been facilitated by a rapid increase in the computational capabilities of the edge nodes over the recent past, and the availability of high-performance mobile GPUs (and specialized toolkits such as CUDA[1] from Nvidia) which can be very effectively utilized for fast matrix inversion operations and complex multiplications.

Furthermore, the observation that the computational complexity for LP-RZF is independent of the number of UTs would imply that the APs (serving as the edge node) need not be upgraded and/or re-configured with an increase in the user count.

6. Conclusion

In Cell-Free Large-Scale MU-MIMO, it is assumed that all the UTs are being served by all the APs in the same time-frequency resource. The signal processing is then performed and administered by the CPU with unlimited fronthaul capacity. These characteristics make a system more complex, unscalable, and impractical. In order to reduce the load on the fronthaul connections, local distributed detection schemes are considered in this paper with realistic and practical system considerations. The results demonstrate that for various distributed configurations, Local-Partial RZF provides the highest achieved average SE while the distributed MR offers the lowest performance. Further, the performance of the distributed schemes can be substantially enhanced by deploying LSFD as a second stage of data detection at the CPU. Moreover, in terms of computational complexity, the Local-Partial RZF distributed scheme can achieve less complexity than the centralized schemes since that the computational complexity in the Local-Partial RZF is independent of the UTs, so it does not grow as $K \to \infty$. The distributed combining scheme has the potential to reduce the interference from other UTs in a distributed manner.

References

1. E. Björnson, L. Sanguinetti, H. Wymeersch, J. Hoydis and T. L. Marzetta, "Massive MIMO is a reality—What is next? Five promising research directions for antenna arrays" Digital Signal Processing. 2019 Nov. 1;94:3-20.
2. M. Shafi et al., "5G: A tutorial overview of standards, trials, challenges, deployment, and practice," IEEE J. Sel. Areas Commun., vol. 35, no. 6,pp. 1201–1221, 2017
3. C. Wang, J. Bian, J. Sun, W. Zhang and M. Zhang. A Survey of 5G Channel Measurements and Models. IEEE Communications Surveys & Tutorials, 2018; 20(4):3142-3168.
4. Z. Lin et al., "Refracting RIS-Aided Hybrid Satellite-Terrestrial Relay Networks: Joint Beamforming Design and Optimization," *in IEEE Transactions on Aerospace and Electronic Systems*, vol. 58, no. 4, pp. 3717-3724, Aug. 2022.
5. Silva, Mário Marques da, and João Guerreiro. 2020. "On the 5G and Beyond" Applied Sciences 10, no. 20: 7091. https://doi.org/10.3390/app10207091.
6. Z. Lin et al., "SLNR-based Secure Energy Efficient Beamforming in Multibeam Satellite Systems," *in* IEEE Transactions on Aerospace and Electronic Systems, 2022.
7. Rappaport, T.S.; Sun, S.; Mayzus, R.; Zhao, H.; Azar, Y.; Wang, K.; Wong, G.N.; Schulz, J.K.; Samimi, M.; Gutierrez, F. Millimeter Wave Mobile Communications for 5G Cellular: It Will Work!, IEEE Access 2013, 1, 335–349.
8. S. Han, C. I, Z. Xu and C. Rowell, "Large-scale antenna systems with hybrid analog and digital beamforming for millimeter wave 5G," in IEEE Communications Magazine, vol. 53, no. 1, pp. 186-194, January 2015.
9. Z. Lin, M. Lin, J. -B. Wang, T. de Cola and J. Wang, "Joint Beamforming and Power Allocation for Satellite-Terrestrial Integrated Networks With Non-Orthogonal Multiple Access," in IEEE Journal of Selected Topics in Signal Processing, vol. 13, no. 3, pp. 657-670, June 2019.
10. L. Dai, B. Wang, Y. Yuan, S. Han, C. I and Z. Wang, "Non-orthogonal multiple access for 5G: Solutions challenges opportunities and future research trends", IEEE Commun. Mag., vol. 53, no. 9, pp. 74-81, Sep. 2015.
11. Z. Lin, M. Lin, T. de Cola, J. -B. Wang, W. -P. Zhu and J. Cheng, "Supporting IoT With Rate-Splitting Multiple Access in Satellite and Aerial-Integrated Networks," in IEEE Internet of Things Journal, vol. 8, no. 14, pp. 11123-11134, 15 July15, 2021.

[1] https://developer.nvidia.com/cuda-toolkit

12. T. L. Marzetta. Noncooperative Cellular Wireless with Unlimited Numbers of Base Station Antennas. IEEE Transactions on Wireless Communications. 2010;9(11):3590-3600.
13. F. Rusek et al., "Scaling Up MIMO: Opportunities and Challenges with Very Large Arrays," *in IEEE Signal Processing Magazine*, vol. 30, no. 1, pp. 40-60, Jan. 2013.
14. H. Q. Ngo, E. G. Larsson and T. L. Marzetta. Energy and Spectral Efficiency of Very Large Multiuser MIMO Systems. IEEE Transactions on Communications. 2013; 61(4):1436-1449.
15. E. G. Larsson, O. Edfors, F. Tufvesson, and T. L. Marzetta, "Massive MIMO for next-generation wireless systems," in IEEE Communications Magazine. 2014; 52(2):186-195.
16. J. Hoydis, S. ten Brink and M. Debbah, "Massive MIMO in the UL/DL of cellular networks: How many antennas do we need?", *IEEE J. Sel. Areas Commun.*, vol. 31, no. 2, pp. 160-171, Feb. 2013.
17. Emil Björnson; Jakob Hoydis; Luca Sanguinetti, Massive MIMO Networks: Spectral, Energy, and Hardware Efficiency. Foundations and Trends in Signal Processing. 2017;11(3-4):154-655.
18. A. Alammari, A, Sharique, M. Spatial channel correlation for local scattering with linear MMSE-based estimator and detector in multi-cell large scale MU-MIMO networks. Trans Emerging Tel Tech. 2021; 32(12):e4366. https://doi.org/10.1002/ett.4366
19. R. Irmer et al., "Coordinated multipoint: Concepts performance and field trial results", *IEEE Commun. Mag.*, vol. 49, no. 2, pp. 102-111, Feb. 2011.
20. D. Wang, J. Wang, X. You, Y. Wang, M. Chen and X. Hou, "Spectral efficiency of distributed MIMO systems", *IEEE J. Sel. Areas Commun.*, vol. 31, no. 10, pp. 2112-2127, Oct. 2013.
21. G. N. Kamga, M. Xia and S. Assa, "Spectral-efficiency analysis of massive MIMO systems in centralized and distributed schemes", *IEEE Trans. Commun.*, vol. 64, no. 5, pp. 1930-1941, May 2016.
22. H. Q. Ngo, A. Ashikhmin, H. Yang, E. G. Larsson and T. L. Marzetta, "Cell-free massive MIMO versus small cells", *IEEE Trans. Wireless Commun.*, vol. 16, no. 3, pp. 1834-1850, Mar. 2017.
23. W. Liu, S. Han, C. Yang, and C. Sun, "Massive MIMO or small cell network: Who is more energy efficient?," *in Proc. of IEEE Wireless Communications and Networking Conference Workshops (WCNCW),* 2013, pp. 24–29.
24. S. Buzzi, C. D'Andrea and C. D'Elia, "User-Centric Cell-Free Massive MIMO with Interference Cancellation and Local ZF Downlink Precoding," *2018 15th International Symposium on Wireless Communication Systems (ISWCS)*, 2018, pp.1-5.
25. A. A. Alammari, M. Sharique and A. A. Moinuddin, "User-Centric Cell-Free and Co-Located Cellular Large Scale MU-MIMO Systems: A Comparative Performance Study With Spatial Channel Correlation in Dense Urban Scenario," *in IEEE Access*, vol. 10, pp. 48792-48809, 2022, doi: 10.1109/ACCESS.2022.3172290.
26. E. Björnson and L. Sanguinetti, "Making Cell-Free Massive MIMO Competitive With MMSE Processing and Centralized Implementation," in *IEEE Transactions on Wireless Communications*, vol. 19, no. 1, pp. 77-90, Jan. 2020.
27. G. Interdonato, E. Björnson, H. Q. Ngo, P. Frenger and E. G. Larsson, "Ubiquitous cell-free massive MIMO communications", *EURASIP J. Wireless Commun. Netw.*, vol. 2019, no. 1, pp. 197, Dec. 2019.
28. Z. Chen and E. Björnson, "Channel Hardening and Favorable Propagation in Cell-Free Massive MIMO With Stochastic Geometry," in *IEEE Transactions on Communications*, vol. 66, no. 11, pp. 5205-5219, Nov. 2018.
29. E. Nayebi, A. Ashikhmin, T. L. Marzetta and H. Yang, "Cell-free massive MIMO systems", *Proc. 49th Asilomar Conf. Signals Syst. Comput.*, pp. 695-699, Nov. 2015.
30. E. Nayebi, A. Ashikhmin, T. L. Marzetta, H. Yang and B. D. Rao, "Precoding and Power Optimization in Cell-Free Massive MIMO Systems," in *IEEE Transactions on Wireless Communications*, vol. 16, no. 7, pp. 4445-4459, July 2017.
31. M. Bashar, K. Cumanan, A. G. Burr, M. Debbah and H. Q. Ngo, "Enhanced max-min SINR for uplink cell-free massive MIMO systems", *Proc. IEEE ICC*, pp. 1-7, May 2018.
32. M. Bashar, K. Cumanan, A. G. Burr, H. Q. Ngo and M. Debbah, "Cell-free massive MIMO with limited backhaul", *Proc. IEEE Int. Conf. Commun.*, May 2018.
33. Ö. T. Demir, E. Björnson and L. Sanguinetti, "Foundations of user-centric cell-free massive MIMO", *Found. Trends Signal Process.*, vol. 14, no. 3, pp. 162-472, 2021.
34. A. Papazafeiropoulos, P. Kourtessis, M. D. Renzo, S. Chatzinotas and J. M. Senior, "Performance analysis of cell-free massive MIMO systems: A stochastic geometry approach", *IEEE Trans. Veh. Technol.*, vol. 69, no. 4, pp. 3523-3537, Apr. 2020.
35. M. Bashar, K. Cumanan, A. G. Burr, , M. Debbah, and H. Q. Ngo, "Enhanced max-min SINR for uplink cell-free Massive MIMO systems," in Proc. IEEE ICC, May 2018, pp. 1–6.
36. T. H. Nguyen, T. K. Nguyen, H. D. Han and V. D. Nguyen, "Optimal Power Control and Load Balancing for Uplink Cell-Free Multi-User Massive MIMO," in *IEEE Access*, vol. 6, pp. 14462-14473, 2018.
37. Z. H. Shaik, E. Björnson and E. G. Larsson, "MMSE-Optimal Sequential Processing for Cell-Free Massive MIMO With Radio Stripes," in *IEEE Transactions on Communications*, vol. 69, no. 11, pp. 7775-7789, Nov. 2021.
38. J. Zhang, J. Zhang, D. W. K. Ng, S. Jin and B. Ai, "Improving Sum-Rate of Cell-Free Massive MIMO With Expanded Compute-and-Forward," in *IEEE Transactions on Signal Processing*, vol. 70, pp. 202-215, 2022.
39. P. Liu, K. Luo, D. Chen, and T. Jiang, "Spectral efficiency analysis of cell-free massive MIMO systems with zero-forcing detector," *IEEE Trans. Wireless Commun.*, vol. 19, no. 2, pp. 795–807, Feb. 2020.
40. S. Buzzi and C. D'Andrea, "Cell-Free Massive MIMO: User-Centric Approach," in *IEEE Wireless Communications Letters*, vol. 6, no. 6, pp. 706-709, Dec. 2017.

41. G. Interdonato, P. Frenger and E. G. Larsson, "Scalability Aspects of Cell-Free Massive MIMO," *ICC 2019 - 2019 IEEE International Conference on Commun. (ICC)*, pp. 1-6, 2019.
42. L. D. Nguyen, T. Q. Duong, H. Q. Ngo and K. Tourki, "Energy efficiency in cell-free massive MIMO with zero-forcing precoding design", *IEEE Commun. Lett*., vol. 21, no. 8, pp. 1871-1874, Aug. 2017.
43. G. Femenias and F. Riera-Palou, "Cell-Free Millimeter-Wave Massive MIMO Systems With Limited Fronthaul Capacity," in *IEEE Access*, vol. 7, pp. 44596-44612, 2019.
44. G. Interdonato, M. Karlsson, E. Björnson and E. G. Larsson, "Local Partial Zero-Forcing Precoding for Cell-Free Massive MIMO," *in IEEE Transactions on Wireless Communications*, vol. 19, no. 7, pp. 4758-4774, July 2020.
45. J. Zhang, J. Zhang, E. Björnson and B. Ai, "Local partial zero-forcing combining for cell-free massive MIMO systems", *IEEE Trans. Commun.*, vol. 69, no. 12, pp. 8459-8472, Sep. 2021.
46. E. Björnson, J. Hoydis and L. Sanguinetti, "Massive MIMO networks: Spectral energy and hardware efficiency", *Found. Trends Signal Process.*, vol. 11, no. 3, pp. 154-655, 2017.
47. E. Björnson, E. G. Larsson and M. Debbah, "Massive MIMO for Maximal Spectral Efficiency: How Many Users and Pilots Should Be Allocated?" in *IEEE Transactions on Wireless Communications*, vol. 15, no. 2, pp. 1293-1308, Feb. 2016.
48. S. -N. Jin, D. -W. Yue and H. H. Nguyen, "Spectral and Energy Efficiency in Cell-Free Massive MIMO Systems Over Correlated Rician Fading," in *IEEE Systems Journal*, vol. 15, no. 2, pp. 2822-2833, June 2021.
49. M.S. Ansari, et al. "Security of distributed intelligence in edge computing: Threats and countermeasures." *The Cloud-to-Thing Continuum*. Palgrave Macmillan, Cham, 2020. 95-122.